

# Photon-assisted electron transport in monolayer graphene with Terahertz wave fields

HAIYANG CHEN\*, CAIJUAN PAN

*School of materials science and Engineering, Baise University, Guangxi 533000, China*

We studied the transport properties of charge carriers in monolayer graphene-based barrier structures with Terahertz wave fields. The angularly averaged conductivity, shot noise, and Fano factor of the system have been calculated and analyzed as the external field strength, incident energy and the barrier width are changed. We find that they are improved and show peculiar behavior, due to the presence of external field. One can control the transport of carriers by adjusting the external field strength and the structure parameters of the system.

(Received October 5, 2018; accepted August 20, 2019)

*Keywords:* Transmission probability, Conductivity, Shot noise, Fano factor

## 1. Introduction

Since the discovery of graphene (a single atomic sheet of graphite), there is great interest both experimentally and theoretically for the investigation of electron transport in graphene [1-7]. Graphene is a single layer of carbon atoms densely packed in a honeycomb lattice, or it can be seen as an individual atomic plane pulled out of bulked graphite or unrolled single-wall carbon nanotubes. Its low-energy dynamics of quasiparticles equivalent to the relativistic fermions, are formally described by the Dirac-like Hamiltonian

$$\hat{H}_0 = -i\hbar v_F \sigma \cdot \nabla \quad (1)$$

Here  $v_F \approx 10^6$  m/s is the Fermi velocity, and  $\sigma = (\sigma_x, \sigma_y)$  are the Pauli matrices. Near the Brillouin zone the graphene is the linear energy spectrum  $E = \hbar v_F k$ . The chiral nature of the particles and linear energy spectrum make the graphene exist a number of unique electronic and transport properties such as an unconventional Hall effect [8,9], special Andreev reflection [10], finite minimal electrical conductivity [8,11]. Klein paradox predicts that relativistic electron can pass through the high potential barrier to approach the perfect transmission in contrast to the conventional nonrelativistic tunneling, and on the nonrelativistic conditions, the transmission probability exponentially decays with the increasing of the barrier height [12,13] and so on.

Now it was allowed to study the possibility of photon-assisted tunneling (PAT) due to the band structure and engineering of confinement potential. According to the experiments on the tunneling between superconducting films in the presence of microwave fields, Dayem and Martin reported evidences of emission or absorption of photons by a single tunneling electron [14]. Tien and Gordon explained qualitatively the multiphoton-assisted electron tunneling current in superconducting diodes [15]. In the presence of an external field  $V \cos \omega t$ , an electron

of energy  $E$  without external field give rise to many sidebands which have energies  $E, E \pm \hbar\omega, E \pm 2\hbar\omega, \dots$ , respectively, due to the exchange of energy between the electrons and the external field. The fluctuation spectrum in the presence of oscillating voltages applied to the

contacts of the sample was obtained by Pedersen and Buttiker [16]. Trauzettel, Blanter et al. studied Photon-assisted electron transport in ballistic graphene by scattering theory [17]. Zeb et al studied the transport of chiral massless electrons in monolayer graphene through a single barrier that is oscillating harmonically in time, and the results show the tunneling to exhibits peculiar behavior with the change of system parameters. They find at normal and close to normal incidence the system show perfect transmission (Klein tunnelings) due to chiral nature of the particles [18]. Rezanian H. and Azizi F. studied the behaviors of both dynamical and static charge susceptibilities of undoped armchair graphene nanoribbon using the Green's function approach in the context of tight binding model Hamiltonian [19]. Lu investigated the transport property of electron in graphene-based double-barrier structure with a time periodic field [20]. Yan investigated graphene multiple p-n junctions and superlattices driven by linear potential [21]. In the previous research work, Chen studied the transport properties of monolayer graphene-based double-barrier (well) structures with a time-periodic potential, and applied the scattering approach to study the transport properties of charge carriers through single layer graphene in the presence of a time-periodic potential, and some general theoretical results are obtained [22,23]. In a series of papers, Wagner studied photon-assisted transport through quantum barriers and wells with driving  $V \cos \omega t$  based on a transfer-matrix formalism [24].

Shot noise is a consequence of the quantization of the charge. With the development of single electron devices, shot noise is paid more and more attention by people, as it will influence the performance of the devices. At the same

time, by research shot noise, one can find out the transport mechanism of a mesoscopic system, and obtain more information than conductance, for example, one can determine the charge and statistics of the quasiparticles relevant for transport and so on [25]. The Schottky's formula  $S_p = 2e \langle I \rangle$  relating to Poissonian shot noise, corresponds to the Poissonian distribution in a macroscopic system [26]. The Fano factor was defined as the shot noise spectral density  $S$  divided by  $S_p$  i.e.,  $F = S / S_p$ , it describes the type of shot noise deviating from the Poissonian one. Shot noise is divided to the Sub-Poissonian ( $F < 1$ ), Poissonian ( $F = 1$ ), Super-Poissonian ( $F > 1$ ) types [27].

In this paper, we investigate the transport properties of monolayer graphene with terahertz wave fields (Terahertz wave usually refers to electromagnetic wave with frequency of 100 GHz-10 THz and corresponding wavelength of 3 mm -30  $\mu\text{m}$ , which is between millimeter wave and infrared light. THz wave is in the special band from electronics to photonics, and it is also the transition region from macroscopic classical theory to microscopic quantum theory) [28,29]. The transmission probability, angularly averaged conductivity, shot noise and Fano factor are studied numerically. The transport properties of graphene exhibits peculiar behavior, due to the presence of an time-periodic potential, and the conductivity, shot noise and Fano factor will be improved. With the increase of the

$\alpha(\alpha = \frac{V_1}{\hbar\omega})$  and the change of structure parameters, the shot noise, Fano factor are enhanced. The transport properties of the system can be controlled by adjusting the structure parameters. Finally, we will give some concluding and prospects.

## 2. Theory and model

We use the same setup in Refs. [18]. A monolayer graphene sheet in the  $xy$  plane. The square potential barrier is set up in the  $x$  direction while carriers are free in the  $y$  direction. The width of barrier is  $a$ , the height of the static square potential barrier is  $V_1$ , oscillating sinusoidally with amplitude  $V_1$  and frequency  $\omega$ , respectively.

Charge carriers with energy  $E$  are incident from one side of the barrier in graphene with an angle  $\phi_0$  with the  $x$  axis the Hamiltonian  $H$  of the system is as follows:

$$H = H_0 + H_1 \quad (2)$$

where

$$H_0 = -i\hbar v_F \sigma \cdot \nabla + V, H_1 = V_1 \cos(\omega t)$$

By solving the Dirac equation in the absence of the oscillating potential [13], we can obtain the wave functions as the incoming wave toward the double-barrier from the left ( $\psi_z(x, y, E, t)$ )

$$\begin{aligned} \psi_z(x, y, E, t) = & e^{ik_y y} \sum_{l=-\infty}^{\infty} [A_{z,l} \begin{pmatrix} 1 \\ s_{z,l} e^{i\phi_{z,l}} \end{pmatrix} e^{ik_{z,l} x} + (1 - \delta_{z,3}) B_{z,l} \begin{pmatrix} 1 \\ -s_{z,l} e^{-i\phi_{z,l}} \end{pmatrix} e^{-ik_{z,l} x}] e^{-i(E + \hbar\omega)t/\hbar} \\ & \times [\delta_{z,2} \sum_{m=-\infty}^{\infty} J_m(\frac{V_1}{\hbar\omega}) e^{-im\hbar\omega t/\hbar} + (1 - \delta_{z,2})] \end{aligned} \quad (3)$$

where  $k_{z,l}$ ,  $k_y$  are the wave vectors along  $x$  and  $y$  direction, respectively,  $J_m(\frac{V_1}{\hbar\omega})$  is the  $m$  th-order Bessel function,  $\delta_{z,2}, \delta_{z,3}$  is the Dirichlet function.  $z=1,2,3$ , representing different regions  $x < 0$ ,  $0 < x < a$ ,  $x > a$ , respectively. In region  $I(z=1)$ ,  $A_{1,l} = \delta_{0,l}$ , and the reflection amplitude  $r_l = B_{1,l}$ , the transmission amplitude

$$t_l = A_{3,l}. \text{ And } s_{1,l} = s_{3,l} = \text{sgn}(E + \hbar\omega), k = \frac{E}{\hbar v_F}, s_{2,l} = \text{sgn}(E - V + \hbar\omega)$$

$$k_{1,l} = k_{3,l} = \sqrt{(\frac{E + \hbar\omega}{\hbar v_f})^2 - k_y^2},$$

$$k_y = E \sin \phi, k_{2,l} = \sqrt{(\frac{E - V + \hbar\omega}{\hbar v_f})^2 - k_y^2},$$

$$\phi_{1,l} = \phi_{3,l} = \tan^{-1}(\frac{k_y}{k_{1,l}}), \phi_{2,l} = \tan^{-1}(\frac{k_y}{k_{2,l}}).$$

Applying the continuity of the wave function at the boundaries

$x=0, a$ , i.e.,  $\psi_1(0, y, E, t) = \psi_2(0, y, E, t)$ ,  $\psi_2(a, y, E, t) = \psi_3(a, y, E, t)$  we obtain the coupled equations in form of infinite series.

$$\delta_{0,n} + B_{1,n} = A_{2,n} + B_{2,n} \quad (4)$$

$$\delta_{0,n} e^{i\phi_{1,n}} - s_{1,n} B_{1,n} e^{-i\phi_{1,n}} = s_{2,n} (A_{2,n} e^{i\phi_{2,n}} - B_{2,n} e^{-i\phi_{2,n}}), \quad (5)$$

$$(A_{2,n} e^{ik_{2,n}a} + B_{2,n} e^{-ik_{2,n}a}) = \sum_{l=-\infty}^{\infty} (A_{3,l} e^{ik_{3,l}a} + B_{3,l} e^{-ik_{3,l}a}) J_{n-l}(\frac{V_1}{\hbar\omega}), \quad (6)$$

$$\begin{aligned} & s_{2,n} (A_{2,n} e^{i\phi_{2,n}} e^{ik_{2,n}a} - B_{2,n} e^{-i\phi_{2,n}} e^{-ik_{2,n}a}) \\ & = \sum_{l=-\infty}^{\infty} s_{3,l} (A_{3,l} e^{i\phi_{3,l}} e^{ik_{3,l}a} - B_{3,l} e^{-i\phi_{3,l}} e^{-ik_{3,l}a}) \times J_{n-l}(\frac{V_1}{\hbar\omega}), \end{aligned} \quad (7)$$

By truncate these equations into finite number of terms starting from  $-N$  to  $N$  ( $N > \frac{V_1}{\hbar\omega}$ ) [18], the transmission

probability for the  $n$ -th sideband  $T_n$  is obtained numerically.

For the zero-frequency component, according to Büttiker formula [30], at zero-temperature the angularly averaged conductivity in this system is given by

$$G = G_0 \sum_{n=-\infty}^{\infty} \int_{-\pi/2}^{\pi/2} T_n \cos[\phi_0] d\phi_0 \quad (8)$$

The shot noise ( $S$ ) and Fano factor ( $F$ ) in the system can be expressed as [31]

$$S = S_0 \sum_{n=-\infty}^{\infty} \int_0^{\pi/2} T_n (1 - T_n) \cos[\phi_0] d\phi_0 \quad (9)$$

and

$$F = \frac{\sum_{n=-\infty}^{\infty} \int_{-\pi/2}^{\pi/2} T_n \cos[\phi_0] d\phi_0}{\sum_{n=-\infty}^{\infty} \int_{-\pi/2}^{\pi/2} T_n (1 - T_n) \cos[\phi_0] d\phi_0} \quad (10)$$

where  $G_0 = \frac{e^2 m v_F W}{\hbar^2}$ ,  $S_0 = \frac{16e^3 V}{h} \frac{EW}{\pi \hbar v_F}$  respectively

$G_0$ ,  $S_0$  are the units of conductance and shot noise,  $E$  is the energy of the incident electron,  $W$  is the width of the graphene sheet. Substitute  $T_n$  into Eqs.(8),(9),(10), the conductivity, shot noise, and Fano parameter for the barrier structures with a time-periodic potential can be obtained by the numerical calculations.

### 3. Numerical results and discussion

Now we express the numerical results for the Dirac electrons in the graphene. The following parameters were used. The incidence electron wave length is  $\lambda = 50 \text{ nm}$ , the barrier wide is  $a = 100 \text{ nm}$ , the barrier height is  $V = -200 \text{ meV}$ , the oscillation frequency is  $\omega = 5 \times 10^{12} \text{ Hz}$

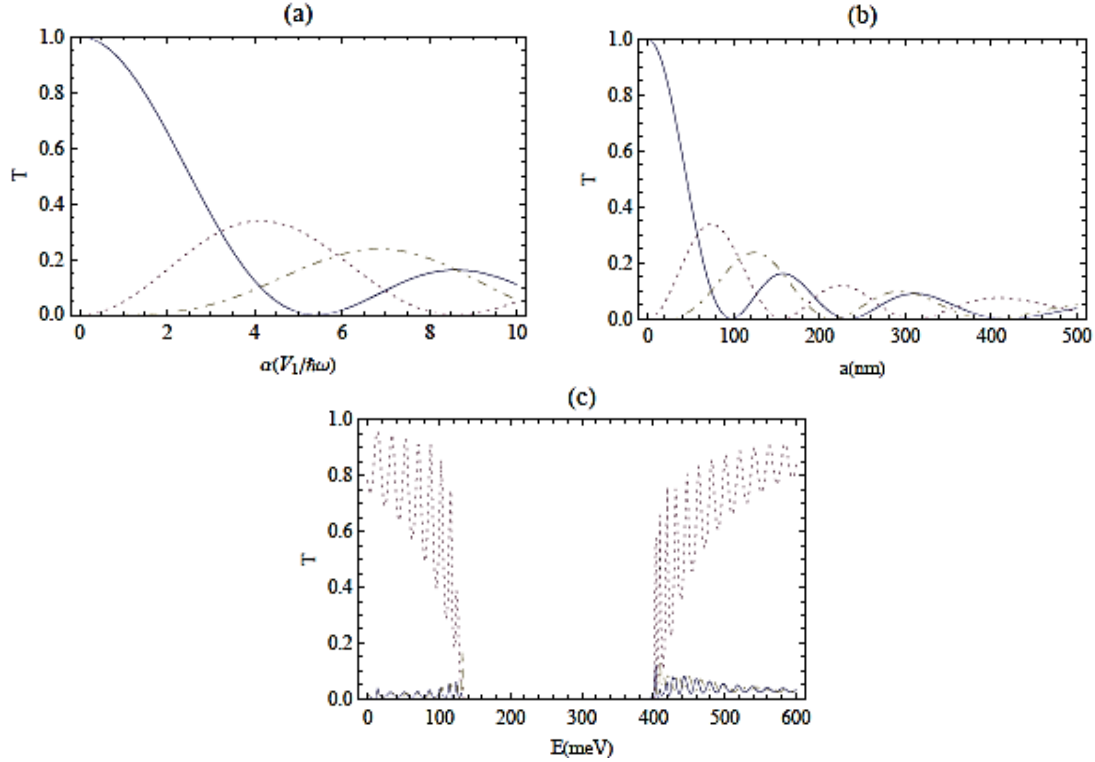


Fig. 1. Transmission probabilities for central band and rstsiebands as a function of (a)  $\alpha$  ( $\alpha = \frac{V_1}{\hbar\omega}$ ), (b) barrier width  $a$ , (c) incident energy  $E$ . For the incident angle  $0^\circ$  ((a) and (b)) and  $30^\circ$  (c). Solid, dotted, dot-dashed line correspond to  $T_0$ ,  $T_{\pm 1}$ ,  $T_{\pm 2}$  ((a) and (b)) and  $T_{-1}$ ,  $T_0$ ,  $T_1$ , respectively

Fig. 1 shows the transmission probabilities for central band and first sidebands as a function of (a)  $\alpha(\alpha = \frac{V_1}{\hbar\omega})$ , (b) barrier width  $a$ , (c) incident energy  $E$ . For the incident angle  $0^\circ$  ((a) and (b)) and  $30^\circ$  (c). Solid, dotted, dot-dashed line correspond to  $T_0$ ,  $T_{\pm 1}$ ,  $T_{\pm 2}$  ((a) and (b)) and  $T_{-1}$ ,  $T_0$ ,  $T_1$ , respectively. One can find that the time-periodic potential contributed side-bands for electron to the graphene, and the transmission probability is spread among the central band and various sidebands. At the same time, the central band  $T_0$  dominates the transmission probabilities for small value of  $\alpha$  and barrier width  $a$ , and the transmission probabilities of various sidebands rise with  $\alpha$  become increasing. Moreover, the total transmission probability is unity due to the Klein tunnelling which is caused by the chirality of the electron, as depicted in Fig. 1(a) and (b). These properties are accordant with previous results in Ref. [18]. The dependence of transmission probabilities on the incident energy  $E$  is shown in Fig. 1 (c). There are two transmission

situations with Klein tunneling and classical motion corresponding to  $E + \hbar\omega > V$  and  $E + \hbar\omega < V$ ,

respectively.  $k_{z,l} = \sqrt{\left(\frac{E - V + \hbar\omega}{\hbar v_f}\right)^2 - k_y^2} < 0$  corresponds to evanescent mode.

Fig. 2 presents the conductivity, shot noise and Fano factor as a function of  $\alpha(\alpha = \frac{V_1}{\hbar\omega})$  with different barrier width. Solid, dotted, dot-dashed line correspond to  $a = 50$  nm; 250 nm, and 400 nm, respectively. We can find that the conductivity, shot noise and Fano factor are flat increase with increasing external field strength  $\alpha$ . The reason is similar to the case of the transmission probability and can be understood by the same way. At the same time, the conductivity, shot noise and Fano factor increase quickly with the increases of the barrier spacing. This can be understood that the large spacing width provide more interaction for electron and external field. Thus, one can control the transport properties of the system by adjusting the structure parameters of the system.

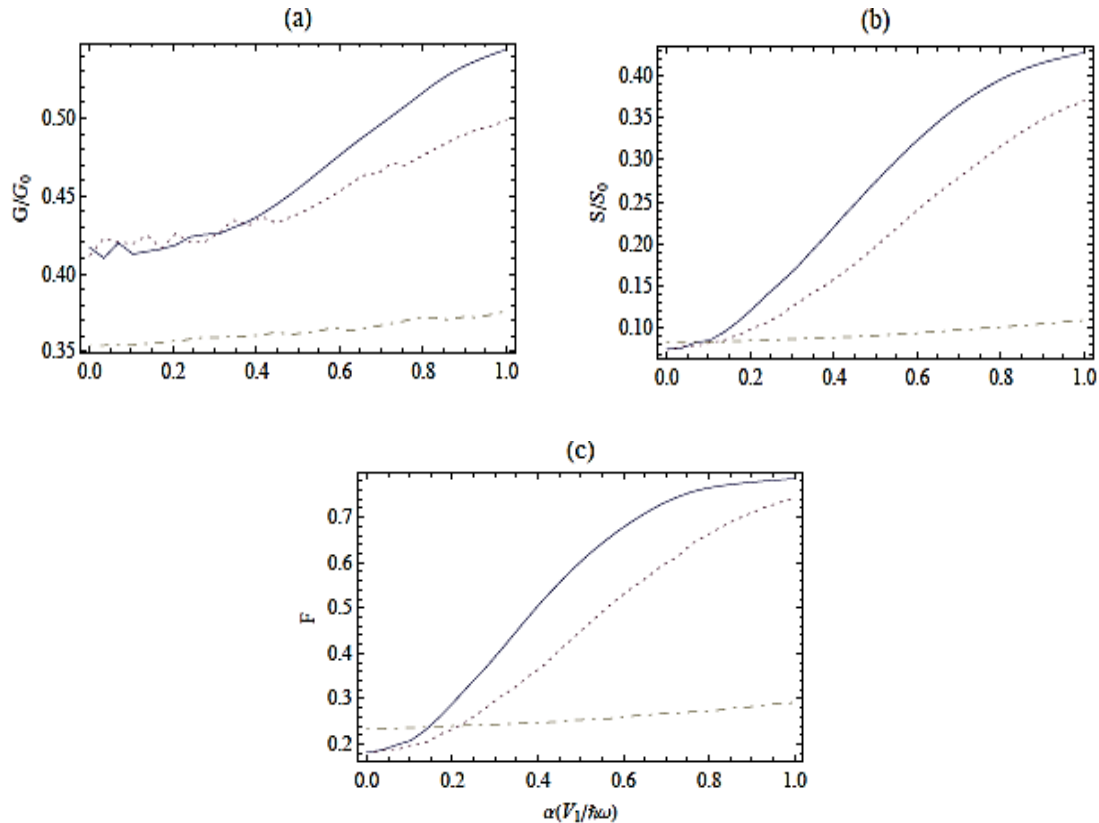


Fig. 2. Conductivity, shot noise and Fano factor as a function of  $\alpha(\alpha = \frac{V_1}{\hbar\omega})$  with different barrier width. Solid, dotted, dot-dashed line correspond to  $a = 50$ nm; 250nm, and 400nm, respectively

Fig. 3 shows the conductivity, shot noise and Fano factor as a function of incident energy. Solid, dotted, dot-dashed lines correspond to  $\alpha=0.8, 0.5, 0$ , respectively. One can find that the conductivity, shot noise and Fano

factor display irregularly oscillatory behavior with increasing energy. This due to that the  $T_n$  is also an oscillating function of the wave vectors  $k_{z,l}$  along  $x$ , and  $k_{z,l}$  is determined by incident energy  $E$ . The other striking

feature is that the conductivity, shot noise and Fano factor remarkably increase with increasing of the external field strength  $\alpha$ , and the change feature keeps the same for them. It implies that the external field plays a important role in the transport properties of the system change. Therefore, we can change transport properties of the system by modulating the external field strength.

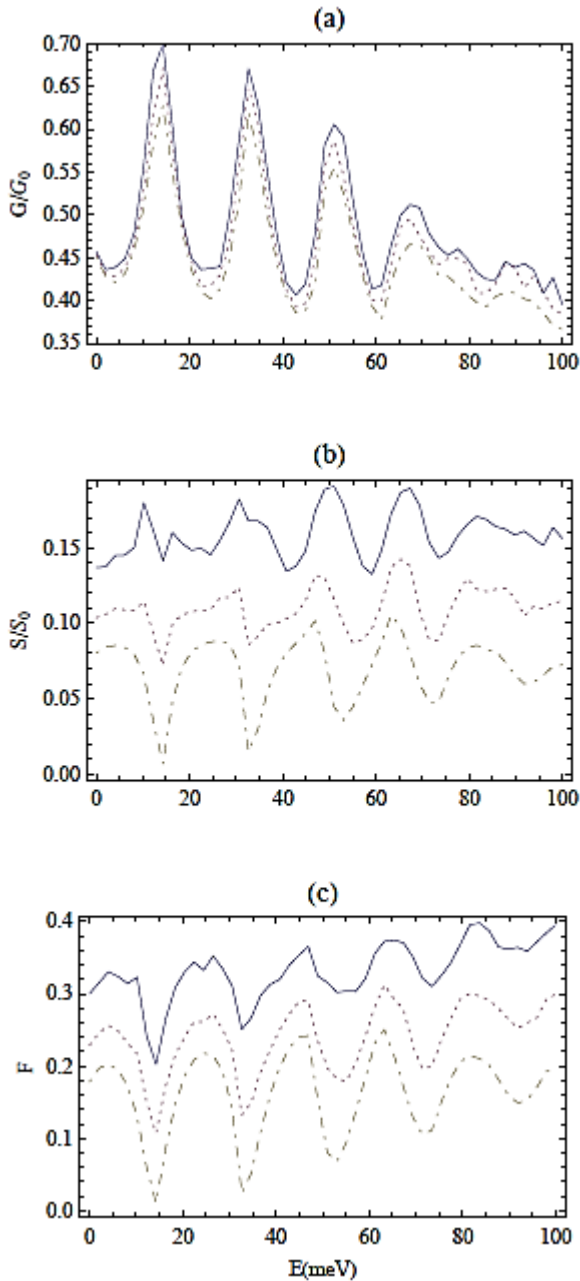


Fig. 3. Conductivity, shot noise and Fano factor as a function of incident energy for solid, dotted, dot-dashed line correspond to  $\alpha=0.8; 0.5; 0$ , respectively

In the Fig. 4, we plotted the conductivity, shot noise and Fano factor as a function of barrier width. The solid, dotted, dot-dashed lines correspond to  $\alpha=0.8, 0.5, 0$ , respectively. It shows that the conductivity, shot noise and Fano factor have oscillating behavior with the change of

barrier width. By comparing the different situations, one can see that because the system is near the static case when the  $\alpha$  is a small value, so the conductivity, shot noise and Fano factor do not change largely, but the external field becomes significant with the increasing of barrier width. Moreover, as can be seen clearly, the shot noise and Fano factor significantly increase with the increasing of external field strength  $\alpha$ . This implies that the transport properties of the system will be more sensitive to external field strength with the increasing of barrier width, and this also shows that  $\alpha$  is significant in determining the transport properties of the system.

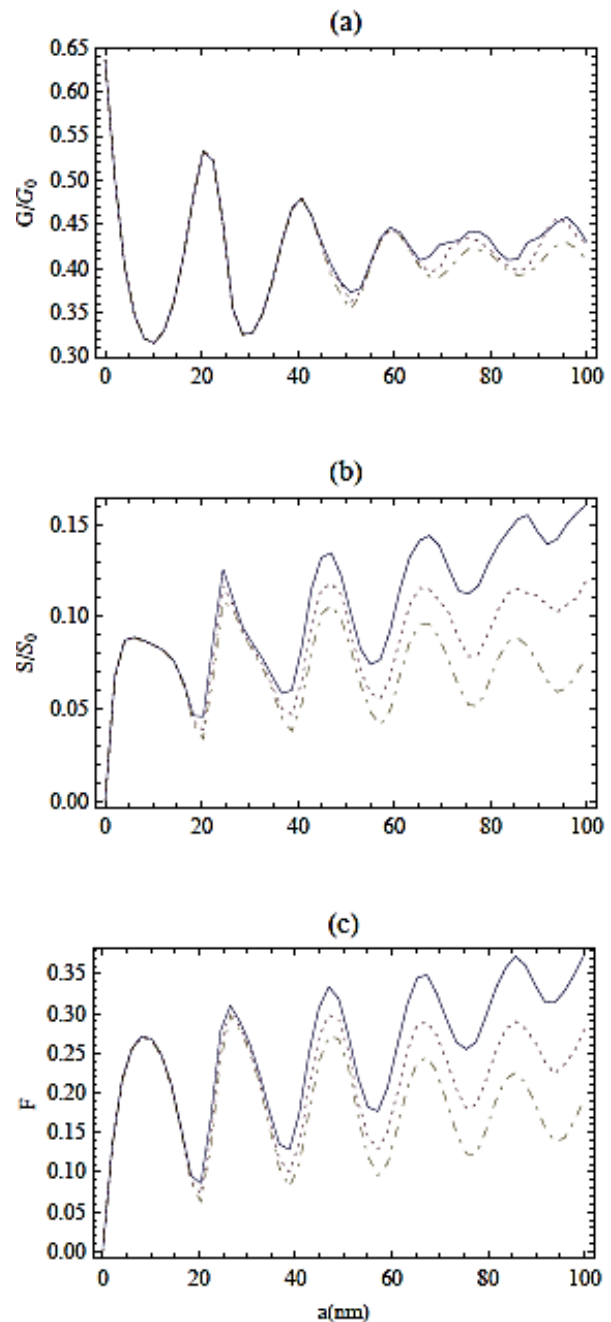


Fig. 4. Conductivity, shot noise and Fano factor as a function of barrier width for solid, dotted, dot-dashed line correspond to  $\alpha = 0.8; 0.5; 0$ , respectively

#### 4. Conclusion

In conclusion, by solving the Dirac equation we obtained the transmission probability of monolayer graphene with a time-periodic potential. We investigated transport properties of the system with the external field strength  $\alpha$  and system parameters including the incident energy, and the barrier width in different cases, respectively. We have found that due to the presence of a time-periodic potential, the transport properties of graphene have peculiar behavior, the conductivity, shot noise and Fano factor are improved. One could control the electron transport by modulating the external field strength and the structure parameters of the system. We hope this work can provide some valuable reference to the design of electron devices relating to the monolayer graphene material.

#### Acknowledgements

This research was supported by the Baise University Science Foundation of China (Grant No. 2015KAN03) and Construction Funds of Master's Degree Granting Units in Guangxi Zhuang Autonomous Region in 2019.

#### References

- [1] Y. Cao et al. *Nature* **556**, 43 (2018).
- [2] K. S. Novoselov, A. K. Geim, S. V. Morozov, D. Jiang, Y. Zhang, S. V. Dubonos, I. V. Grigorieva, A. A. Firsov, *Science* **306**, 666 (2004).
- [3] Y. He, W. Yu, G. J. Ouyang, *Phys. Chem. C* **119**, 5420 (2015).
- [4] S. Kumar, D. Parks, K. Kamrin, *ACS Nano* **10**, 6552 (2016).
- [5] X. M. Wang, H. Tian, M. A. Mohammad, *Nature Commun.* **6**, 7767 (2015).
- [6] S. Goossens, G. Navickaite, C. Monasterio, *Nature Photon.* **11**, 366 (2017).
- [7] Z. F. Liu, *Acta Phys. Chim. Sin.* **33**, 853 (2017).
- [8] K. S. Novoselov, A. K. Geim, S. V. Morozov, D. Jiang, M. I. Katsnelson, I. V. Grigorieva, S. V. Dubonos, A. A. Firsov, *Nature (London)* **438**, 197 (2005).
- [9] Y. Zhang, H. L. Stormer, P. Kim, *Nature (London)* **438**, 201 (2005).
- [10] W. J. Beenakker, *Phys. Rev. Lett.* **97**, 067007 (2006).
- [11] K. S. Novoselov, E. McCann, S. V. Morozov, V. I. Fal'ko, M. I. Katsnelson, U. Zeitler, D. Jiang, F. Schedin, A. K. Geim, *Nature. Phys.* **2**, 177 (2006).
- [12] O. Klein, *Z. Phys.* **53**, 157 (1929).
- [13] M. I. Katsnelson, K. S. Novoselov, A. K. Geim, *Nat. Phys.* **2**, 620 (2006).
- [14] A. H. Dayem, R. J. Martin, *Phys. Rev. Lett.* **8**, 246 (1962).
- [15] P. K. Tien, J. P. Gordon, *Phys. Rev.* **129**, 647 (1963).
- [16] M. H. Pedersen, M. Büttiker, *Phys. Rev. B.* **58**, 12993 (1998).
- [17] B. Trauzettel, Blanter, A. F. Ya Morpurgo, *Phys. Rev. B* **75**, 035305 (2007).
- [18] M. A. Zeb, K. Sabeeh, M. Tahir, *Phys. Rev. B.* **78**, 165420 (2008).
- [19] H. Rezanian, F. Azizi, *Chin. Phys. B* **25**(9), 097303 (2016).
- [20] W. T. Lu, S. J. Wang, *Commun. Theor. Phys.* **56**, 163 (2011).
- [21] W. X. Yan, *Chin. Phys. Lett.* **30**, 047202 (2013).
- [22] H. Y. Chen, *Physica B* **440**, 10 (2014).
- [23] H. Y. Chen, *Phys. Lett. A* **378**, 2226 (2014).
- [24] M. Wagner, *Phys. Rev. Lett.* **76**, 4010 (1996).
- [25] Ya. M. Blanter, M. Büttiker, *Phys. Rep.* **336**, 1 (2000).
- [26] W. Schottky, *Ann. Phys.* **57**, 541 (1918).
- [27] H. K. Zhao, J. Zhang, J. Wang, *Europhys. Lett.* **109**, 18003 (2015).
- [28] Y. Zhang et al., *Acta Phys. Sin.* **66**, 204101 (2017).
- [29] Zh. Zh. Zhang et al., *Acta Phys. Sin.* **67**, 090702 (2018).
- [30] M. Büttiker, *Phys. Rev. B* **46**, 12458 (1992).
- [31] J. Tworzydło, B. Trauzettel, M. Titov, A. Rycerz, C. W. J. Beenakker, *Phys. Rev. Lett.* **96**, 246802 (2006).

\*Corresponding author: chenhaiyang05@126.com